

Diffusion Airfoils), slotted blades, or other methods of boundary layer control helped designers to use higher aerodynamic loads on compressor blades. Tandem blading is one of passive methodology in controlling boundary layer which is based on using the momentum of flow over the pressure side of first blade to avoid the separation on suction surface of the second blade and ultimately achieve higher flow deflection which leads to more aerodynamic loads.

2. LITERATURE SURVEY

In the past 30 years, several experimental investigations together with some numerical studies have been performed on tandem blades. These attempts considered both subsonic and transonic flow regimes. Cheatham (1974) and Brent and Clemmons (1975) designed and tested a tandem blade compressor stage named stage E. flow properties are measured and compressor characteristic maps are reported for uniform and also distorted inlet flow. They also performed a similar study on a conventional compressor stage named stage D. the performance of conventional compressor stage is also reported for both uniform flow and distorted inlet flow. Both stages have been designed for equal rotational speed, equal hub and shroud geometry, similar effective chord length and also equal design DF value. They concluded that tandem stage achieves higher pressure ratio in all rotational speeds. But in lower rotational speeds efficiency of tandem design is lower than conventional design. In 100% and 110% of design rotational speed, efficiency of tandem design is higher than conventional stage. Bammert and Beelte (1980) designed and tested a 4 stage compressor with high degree of reaction. First stage rotor and all stator rows were designed on the basis of single conventional blades but other rotor blades used tandem configuration. In their compressor, stagger angle of stator rows could be varied in order to evaluate the effect of various stagger angles on compressor map. Changing the stator stagger angles resulted in shift of compressor characteristic maps, change of characteristic curve slopes and surge margin. Suga *et al.* (2003) who had primarily designed and tested a subsonic tandem compressor rotor, in their next investigation, they presented the results of a transonic tandem compressor rotor. In their studies, they discussed about optimum configuration of tandem cascade. Flow pattern in the blade passages together with compressor performance maps were reported. McGlumphy *et al.* (2009, 2010) developed a 2D method for designing tandem cascade based on prescribing certain diffusion factor and solidity of tandem cascade. Employing different geometrical parameters and using CFD models, he offered optimum geometrical parameters which provided minimum loss conditions. Using the results of optimum design of 2D blades, he reported the performance of a high hub/tip ratio subsonic tandem rotor in 3D frame. He suggested that, using tandem blades in the rear stages of axial-flow compressors provides specific advantages to achieve high DF

values for blade aerodynamic loading and low loss coefficients. Qiushi *et al.* (2010) carried out a numerical investigation on a tandem stator with supersonic inlet flow. Geometrical parameters were changed and optimum values in each case were reported to achieve minimum loss status. Hoeger *et al.* (2011) designed a high Turning Compressor Tandem Cascade for high subsonic flow regime using CDA profiles. Muller *et al.* (2011) tested and compared the performance of Hoeger's Design. They also compared the tandem cascade with a single blade cascade designed for similar turning angle. Flow pattern and loss parameters were reported for both design and off-design conditions. They showed that at high Mach numbers, the tandem designed cascade achieves lower losses than single blade cascade, but in subcritical flows losses are larger in comparison to single blade cascade. They also concluded that turning is higher in tandem cascade at all tested Mach regimes. Shen *et al.* (2012) used DCA profile blades in their numerical and experimental study of a tandem cascade. They studied the effect of geometrical configurations on loss coefficient of tandem cascade. They also studied the effect of injected flow on the wake formed at the rear side of blades.

3. TANDEM CASCADE GEOMETRICAL REPRESENTATION

Some parameters are required to define the geometry of a tandem blade. These parameters are shown in fig. 1. Similar to conventional blades, chord length (C) and stagger angle (ξ) are defined for both front and aft blades. Subsequently, an effective value for each of these parameters is also introduced for a set of tandem blade.

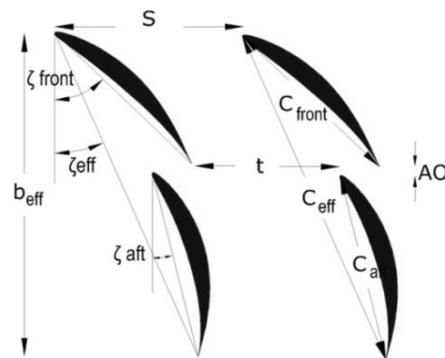


Fig. 1. Geometrical parameterization for tandem cascade.

Effective stagger angle (ξ_{eff}) is the angle between axial reference line and the line connection leading edge of front blade to trailing edge of aft blade. Two important parameters of percentage of axial overlap (%AO) and percent of pitch (%P) show how much the blades overlap each other. These parameters are defined in eq. (1) and eq. (2).

$$\%P = \frac{t}{S} \quad (1)$$

$$\%AO = \frac{AO}{b_{eff}} \quad (2)$$

That, b_{eff} or axial effective chord is defined by eq. (3) as below.

$$b_{eff} = (C_f \cdot \cos \xi_f + C_a \cdot \cos \xi_a - AO) \quad (3)$$

Then, effective chord and effective solidity will be defined respectively by eq. (4) and eq. (5) as below.

$$C_{eff} = \frac{b_{eff}}{\cos \xi_{eff}} \quad (4)$$

$$\sigma_{eff} = \frac{C_{eff}}{S} = \frac{1}{\cos \xi_{eff}} \left((\sigma_f \cos \xi_f + \sigma_a \cos \xi_a) - \frac{AO}{S} \right) \quad (5)$$

In present study, this definition of solidity uses the effect of not only axial overlap (AO) but also it considers the effect of stagger angle as well.

4. DESIGN PROCEDURE

In the current project, the design procedure is on the basis of repeatable velocity triangles of tandem stage at mid blade height shown in fig. 2. Flow enters into the rotor front blades with relative velocity of W_{11} , and leaves the front blade with W_{12} . The relative velocity at entry to aft blade is W_{21} while it leaves rotor row with W_{22} . The front blades of stator receive flow with absolute velocity of C_{21} . The exit velocity is C_{22} at the trailing edge. Flow enters the aft blades of stator with C_{12} and leaves with C_{11} . Described velocity vectors through tandem cascade are shown in fig. 3.

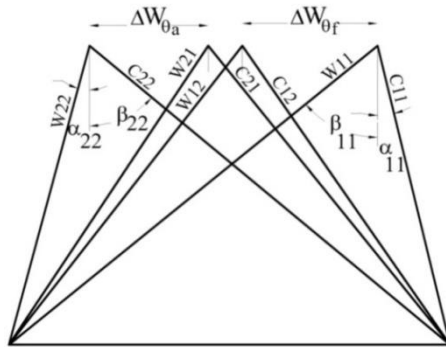


Fig. 2. Tandem cascade velocity triangles.

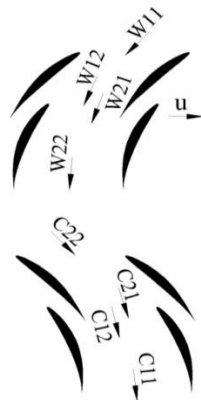


Fig. 3. Velocity vectors through tandem stage cascade.

For non-repeatable velocity triangles, stator outlet velocity vectors will not be equal to rotor absolute

velocity vectors. For repeatable velocity triangles, vector of C_{33} must be equal to C_{11} vector.

McGlumphy *et al.* (2009) suggestion was to use equal aerodynamic load on both front and aft blades. It is also suggested to assume equal values for relative angles at the exit of front rotor and entry to the aft blades, which means that $\beta_{12} = \beta_{21}$. Therefore, the flow angle does not change while passing between front and aft blades. This consideration simplifies the velocity triangles shown in fig. 2. Moreover, if front and aft stator blades are designed in a manner that they turn the flow angles respectively to absolute angles of α_{12} and α_{11} , then repeatable velocity triangles will be achieved. The resultant velocity triangles are shown in fig. 4.

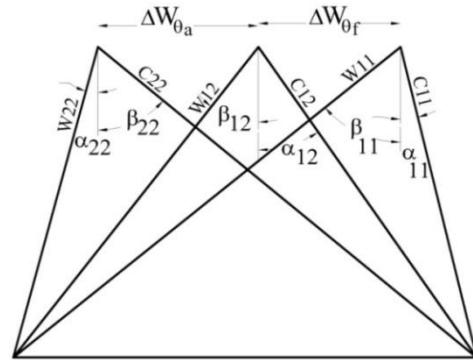


Fig. 4. Simplified tandem cascade velocity triangles.

If one decides on the values of well-known non-dimensional performance parameters of stage loading coefficient (ψ), Flow coefficient (ϕ) and reaction ratio (Λ), then the velocity triangle of tandem blades can be constructed.

Other non-dimensional parameters such as DeHaller number (DH) and diffusion factor (DF) can be calculated individually for both front and aft blades to predict the level of loading and deflection of individual blades. However, their effective values are defined for each tandem blade row to evaluate the overall performance of tandem stage. Using the above notation on velocity triangle these terms are introduced as follows:

$$DH_{f,r} = \frac{W_{12}}{W_{11}} \quad (6)$$

$$DH_{a,r} = \frac{W_{22}}{W_{12}} \quad (7)$$

Effective value of DH for rotor blades will be W_{22}/W_{11} and could be shown as below. It is also worth saying that, since DH number is less than 1.0 for each row, the effective value is much more smaller than 1.0.

$$DH_{eff} = DH_f \times DH_a$$

$$DH_f < 1; DH_a < 1 \quad (8)$$

$$DH_{eff} \ll 1$$

DF for front and aft blades and also its effective value could be derived as below.

$$\begin{aligned}
 DF_f &= \left(1 - \frac{\cos\beta_{11}}{\cos\beta_{12}}\right) + \left(\frac{\cos\beta_{11} \times (\tan\beta_{11} - \tan\beta_{12})}{2\sigma_f}\right) \\
 DF_a &= \left(1 - \frac{\cos\beta_{22}}{\cos\beta_{21}}\right) + \left(\frac{\cos\beta_{22} \times (\tan\beta_{22} - \tan\beta_{21})}{2\sigma_a}\right) \\
 DF_{eff} &= \left(1 - \frac{\cos\beta_{11}}{\cos\beta_{22}}\right) + \left(\frac{\cos\beta_{11} \times (\tan\beta_{11} - \tan\beta_{22})}{2\sigma_{eff}}\right)
 \end{aligned}
 \tag{9}$$

It is also useful to introduce work coefficient which can be written as below.

$$\begin{aligned}
 \psi_f &= \frac{\Delta W_{\theta,f}}{U} \\
 \psi_a &= \frac{\Delta W_{\theta,a}}{U} \\
 \psi_{eff} &= \psi_f + \psi_a
 \end{aligned}
 \tag{10}$$

Experience gained from the past, suggests some limitations on the values of parameters such as stage loading coefficient. These limitations still should be respected, bearing in mind that in the case of tandem blades the values of these non-dimensional parameters increase due to the specific feature of this type of blades.

Once effective stage loading coefficient is decided, it is divided equally between each row and velocity triangles at mid blade height are computed. After that it is customary to make a choice on the distribution of swirl along the blade height which enables the designer to obtain effective values of non-dimensional parameters together with rotor and stator inlet and outlet flow angles (α_{11} , α_{22} , β_{11} and β_{22}) from hub to tip. Dividing ψ for front and aft blades makes it possible to calculate values of intermediate flow angles (α_{12} and β_{12}). At next stage of design procedure, it is possible to use cascade data to predict loss and efficiency of each blade row. Axial overlap and percent pitch values are also among the important parameters that should be decided on. Although a value of 5% for axial overlap and 80% for percent pitch are recommended by McGlumphy *et al.* (2009) and Qiushi *et al.* (2010), but it is important to elaborate the effects of such decisions. The selection of values of axial overlap and percent pitch in three dimensional cases are more critical and need to be justified. This is because, when certain swirl distribution is applied to the flow, blades will eventually twist in the span direction and blades may collide to each other at other radiuses. Having obtained the flow angles, blade angles can be calculated by using certain correlations. Afterward, a method for stacking blades from hub to tip is required to be decided. Blades can be stacked on a straight line, or a curved line. Moreover, the stacking point must be selected on blade profiles. In this respect, a designer's choice can be either of the following strategies:

Strategy I: setting %AO and %P for blade mid height radius and stack profiles on a specified point such as Centroid, leading edge, point of 1/4 of chord and etc. Using this strategy, stacking line will be a straight line and %AO and %P may change from hub to tip due to the three dimensional twist of blades. Of course, on some radii's %AO and %P may deviate from optimum values proposed by

correlations, but blades will stack on an orthogonal line over the machine axis. This could strength blades from the structural point of view.

Strategy II: setting %AO and %P for all radii's, and then stacking blade profiles on a curved line. By using this strategy, the blade will lean. It is possible to keep %AO and %P to optimum values, but surely, manufacturing of such blades need more attention.

Figure 5 shows the whole flow chart of design methodology.

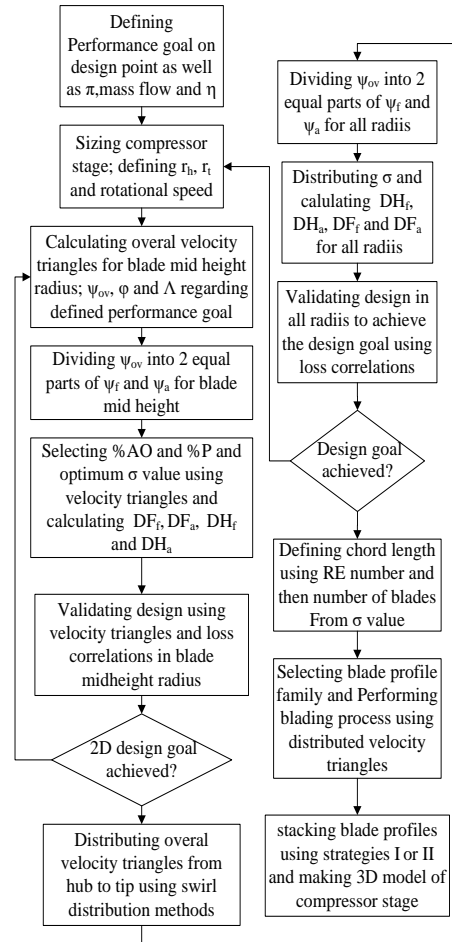


Fig. 5. Tandem compressor stage design procedure.

5. CASE STUDY

Using design procedure described in section 4, a highly loaded tandem compressor stage is designed. In order to compare the performance, another compressor stage is designed with conventional blades with customary design loading coefficients. Both stages are designed to receive axial flow with zero swirl at inlet (α_{11} and α_1 are set to zero) and repeatable velocity triangles (stage inlet and outlet absolute flow angles are equal). Designing the rotor using high value of work coefficient deflects the flow more than a conventional design. To return the flow into the axial direction, the stator experiences higher diffusion process, and to avoid the separation

due to the higher turning angle, the stator is also designed with tandem cascade.

For better comparison of the two stages, geometrical parameters as well as hub and shroud profiles, and effective chord and chord lengths of tandem and conventional stages are set to equal values. Design rotational speed is set also equal too. Both stages are designed for equal values of blade loading parameters as well as DF and DH numbers. Design specifications of tandem and conventional stages are tabulated in Table 1. Non-dimensional parameters are reported for blade mid height radius as well. More detail parameters of both cases are presented in Table 2.

Table 1 Design specifications for compressor stages

Parameter	Value
n_d	9000 rpm
$DH_{r,s}^I$	0.63,0.69
$DF_{r,s}^I$	0.55,0.51
r_{hat} inlet	12 cm
r_t at inlet	24.5 cm
Tip clearance	1.01 mm

Note I : for tandem stage, effective values of parameters are reported.

Table 2 Detailed design parameters for compressor stages

Parameter	Tandem	Conventional
ψ^{II}	0.80	0.49
ϕ^{II}	0.77	0.50
Λ^{II}	0.55	0.74
$\sigma_{eff,r,s}$	1.9, 2.0	1.6, 1.7
$C_{eff,r,s}$	8.73, 10.13cm	-
$C_{r,s}$	5.5 cm	10 cm
$N_{r,s}^{III}$	22,23	17,18

Note II: values are reported for blade mid-height radius.

Note III: number of blades is number of pair sets for tandem design.

In both stages, blade sections are stacked on centroid of blade profile, and a straight line perpendicular to the machine axis is selected as the staking line. For tandem case, strategy I is employed. In the current design, family of NACA65 airfoil profiles with a maximum thickness/chord of 10% is used for both stages. In order to design 3D geometry of blades, a certain distribution of swirl should be decided. In the current design, exponential swirl distribution is selected for both stages.

Figure 6 shows top view of both conventional and tandem designs respectively.

Since, a low hub/tip ratio was selected, high blade height was resulted which consequently caused an extreme twist. In case of Conventional cascade, this decision does not make any problem, but in the case

of tandem blades, rotor blade twist affects the geometrical parameters such as %AO and %P. In other words, proper values of %AO and %P will do not provide a situation that blades collide each other at hub radius. Variation of %AO due to the rotor blade twist is shown in fig. 6. Also, because of less twist in stator blades, it is shown that %AO does not change from hub to tip radii's. Such situation it is possible to keep the %AO and %P to the recommended values. Table 3 shows the values of %AO and %P for hub, mid and tip radii's for the tandem case.

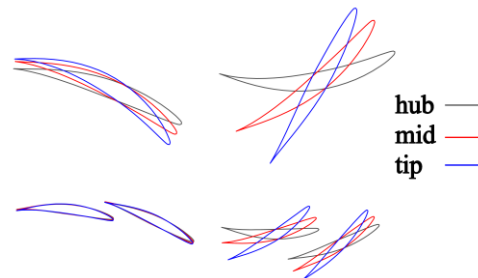


Fig. 6. Top view of tandem and conventional stages.

Table 3 Changes of geometrical parameters due to the radius change.

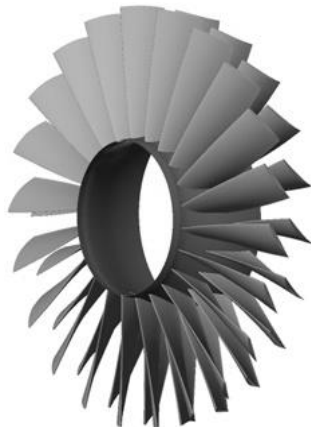
	Rotor		Stator	
	%AO	%P	%AO	%P
Hub	20	82	5	74
Mid	15	51	5	80
Tip	4	50	5	86

In conventional design, extreme twist is also occurred in rotor blades. Twist affects the structural and modal behavior of both tandem and conventional cases. Figure 7 shows final 3D solid views of tandem and conventional rotor designs respectively. In conventional design, extreme twist also occurs too in rotor blades. Twist effect must be considered in structural and modal analysis for both tandem and conventional cases.

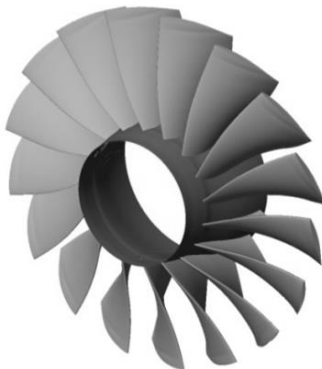
6. NUMERICAL MODEL DEVELOPMENT

3D numerical flow analysis is done with commercial CFD code CFX-5. CFX is a general purpose fluid dynamics solver, that solves the steady and unsteady, compressible and incompressible Reynolds-averaged, navier-stokes (RANS) equations using finite volume approach. CFX uses cell-vertex approach for domain discretization; Primitive variables as well as velocity vector components, pressure and temperature values etc. are stored on corner of elements. RANS Equations are integrated on control volumes. Gauss's theorem is used to exchange the volumetric integrals into surface integrals. Then, a set of algebraic equations is generated to solve values of pressure and velocity vectors. To solve the set of algebraic equations, method of algebraic multigrid is used. In this

method, the equations are firstly solved for a coarse mesh by summing the fine mesh equations, and then CFX refines the mesh for more accurate results.



A: Tandem design



B: Conventional design

Fig. 7. 3D view of compressor rotors.

The frame change is one of the most important parts in turbomachinery flow simulation. CFX uses 3 strategies to connect flow characteristics of rotating and stationary components: Frozen rotor, Stage and Transient rotor-stator. Stage and frozen rotor usually are used for steady state calculations. In frozen rotor modeling, fluxes change through frames, but the relative orientation of machine components does not change. This approach is usually used for first guess or initialization progress.

Stage model uses circumferential averaging of the fluxes through bands on the connecting planes. Steady state results will be available in each reference frame.

The Transient Rotor-Stator is usually used when it is important to simulate interaction effects between rotating and stationary components. This approach needs more CPU-time and computational resources. In this study, Stage approach is used for frame change modeling between rotating and stationary components.

Following boundary conditions are used for all 3D flow simulations in this study

- At inlet, total pressure and total temperature

together with flow direction and turbulent intensity are defined at stage inlet. In all cases, these parameters are set as:

Po1=1 atm, To1=288 K, axial inlet flow and turbulence intensity=5%

- At outlet boundary, average static pressure is set to maximum 1atm.
- Smooth wall for blades, hubs and stator shroud
- Counter rotating wall for rotor shroud

One blade passage is modeled for rotor and stator rows, so rotational periodic interfaces are used for side boundaries of passage block. To obtain performance characteristic of the compressor stage, outlet pressure has been increased gradually until numerical instability observed. Convergence criterion is set to 10^{-5} for RMS residual. Pressure ratio and total to total efficiency values are derived by mass flow averaging procedure from inlet and outlet flow conditions. For turbulence modeling, k- ϵ model with scalable wall function is used.

6.1 Validation

It is vital to validate the developed numerical model so as to ensure the level of accuracy of the results. In this regard, the well-known NASA stage 67 is selected because of the availability of detail geometrical data and vast experimental results on its stage performance characteristics and flow pattern within its stator row (Hathaway, 1986). In addition, a wide domain of flow regimes from subsonic to transonic flow occurs at various rotational speeds in this rotor which can verify the robustness of numerical model. The flow pattern of its isolated rotor row was experimentally measured at its design speed and reported (Strazisar *et al.*, 1989). Experimental and numerical Part-speed Performance characteristic maps are also available (Fidalgo *et al.*, 2012).

The computational domain is discretized by using structured H-type grid in the passages and O-type grid is employed in boundary layer regions to have more accurate results. In order to get ensured of the independency of results to computational grids, three sets of coarse, medium and fine grids are generated. These sets of grids are shown at mid-span height of blades in fig. 8.

More details of computational grids are tabulated in Table 4.

The computations are undertaken at design speed of 16041.8 RPM where stage67 provides a pressure ratio of 1.63 at mass flow rate of 34 kg/s in peak efficiency point. Table 5 compares the results of computations for all three types of grids. Medium grids show a deviation of nearly 0.5% which is sufficiently accurate. 3D flow for design speed is investigated using 3 levels of computational generated grids for stage 67 near peak efficiency point. Mass flow deviation for grid study is reported in Table 5.

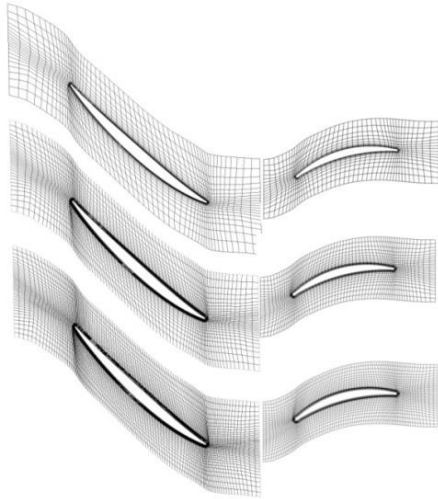


Fig. 8. Mid-span layer of stage 67 computational grids.

Table 4 Computational grid specifications in brief

	Number of nodes	Height layers	O-type layers	Tip layers
Coarse r,s	68k,31k	30	10,5	4,-
Medium r,s	242k,114k	50	16,11	7,-
Fine r,s	653k,321k	80	21,17	11,-

Table 5 grid study results

	mass flow	% deviation
Coarse	34.1570	-
Medium	34.3265	0.496412
Fine	34.3431	0.048355

Figure 9 demonstrates stream-wise pressure distribution at rotor mid span height. Medium and fine grid results are quite similar to each other and it shows that increasing number of grids does not provide further accuracy.

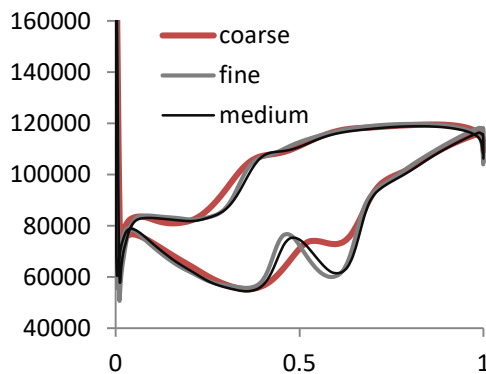


Fig. 9. Stream-wise rotor pressure distribution in mid-span height.

The extensive evaluation of results on other flow parameters proved that medium number of grids is acceptable for doing the rest of calculations; therefore, the results from now are on the basis of medium number of grids. Comparison of experimental and numerical contours of time averaged velocity components are shown in fig. 10.

Absolute value of velocity in stationary frame has been presented. The results correspond to the point of peak efficiency at 50% span of stator blades. There is a good agreement between numerical results and experimental measurements.

In fig. 11, contours of Mach number for isolated rotor row have been shown in 70% span from tip radius. The operating point is near to peak efficiency point at design speed.

A good agreement is seen on both the form of the contours and their values.

Figure 12 compares characteristic performance of NASA 67 stage with the equivalent maps extracted from numerical solution at design speed.

As it is seen, variation of pressure ratio against mass flow rate extracted from both numerical and experimental evaluation coincides with each other, but the safe operation domain is less than the experimental domain. Surge point is nearly 4.88% more and choke point is 1.09% less than the experimental values.

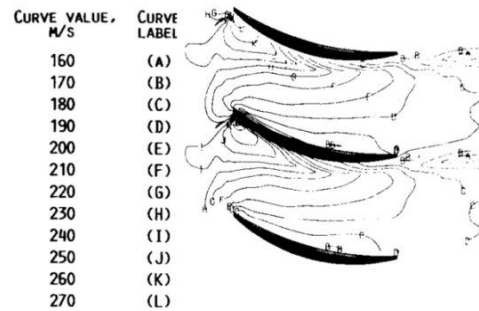
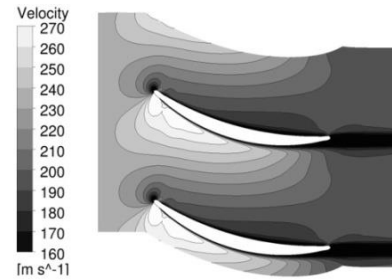


Fig. 10. Comparison between experimental and numerical results of Stator absolute velocity magnitude contours in 50% span.

Pressure ratio obtained from numerical solution is maximum 0.3% less than the experimental value. The authors believe that the results may be improved if a more accurate modeling of frame change between rotor and stator is employed. In the current study, due to the lack of detailed geometrical data, blade fillets at hub radius are ignored. Also in the tip region, the blade is simply truncated. Due to the higher speeds of flow at tip region, the tip clearance shape extremely affects the tip region flow and this could be a source for validation error. For more accurate numerical investigation it is needed to implement a refined geometrical model.

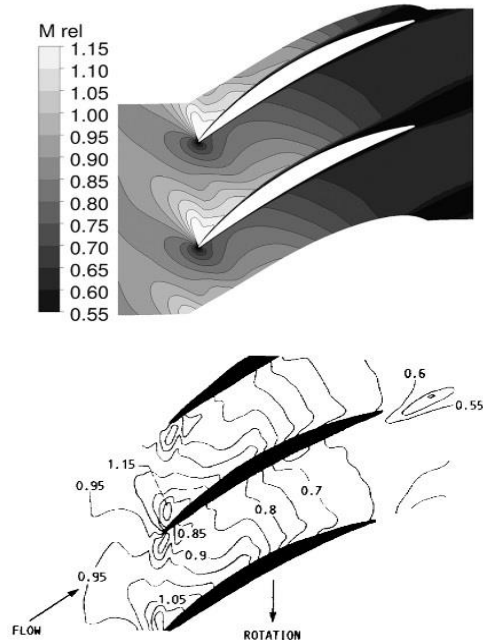


Fig. 11. Comparison between experimental and numerical results of rotor relative Mach number contours in 70% span from tip.

In the case of efficiency, the developed numerical model predicts a very accurate value at design point, but at other mass flow rates it gradually deviates from the experimental values. The maximum deviation in efficiency is evaluated as 1.5% less than experimental values.

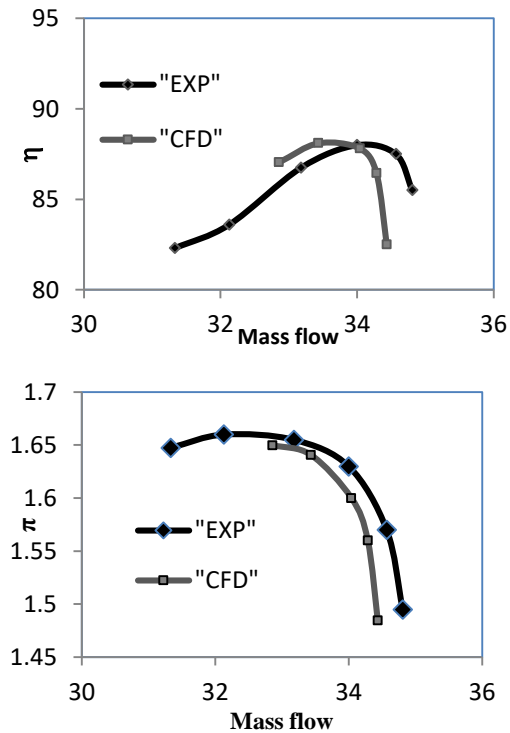


Fig. 12. Comparison of Characteristic map, results of experimental and numerical analysis.

In fig. 13, part-speed performance of isolated rotor

is compared between current study, experimental results and numerical results (Fidalgo *et al.* 2012). Simulations are done for 60%, 70%, 80%, 90% and 100% design speeds.

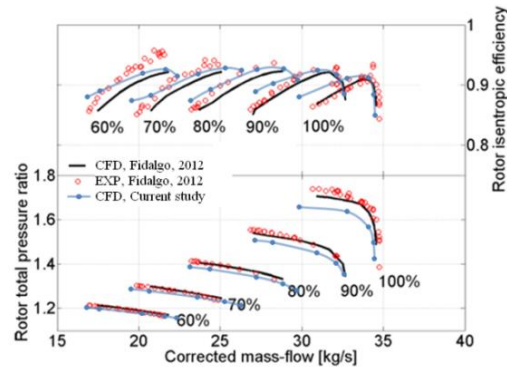


Fig. 13. Part-speed rotor characteristic map.

Apparently, pressure ratio resulted from the current numerical model is in good agreement with experiment especially at lower rotational speeds. At higher speed some deviation is occurred. The pressure ratio maximum deviation is 3.5%. In the current study, mass flow is more accurately predicted by the numerical model. In the case of efficiency, there is also a good agreement between numerical and experimental results especially at maximum mass flow rates and peak efficiency points regions. In near stall regions, numerical model predicts higher values than experiment which is maximum 5%.

Having compared the results of numerical model, it is concluded that the developed model has the required capability to simulate the flow with in both conventional and tandem stages in wide range of rotational speed even at transonic regimes. Although in this study it is mainly focused on subsonic flow.

It must be considered that results of coarse grids are also acceptable in all validation studies, but for more accuracy medium number of grids is chosen for the remaining part of study.

6.2 Case setups

Similar investigation is performed for tandem and conventional design cases. Three sets of computational grids with H-type mesh for passages and O-type mesh round the blades have been generated for both cases. To detect the tip leakage flow on rotor tips, some layers of H-grid are generated in shroud tip region. Grid specifications are briefly tabulated in Table 6. Also mid-span views of grids are shown in fig. 14 and fig. 15, respectively for tandem and conventional cases.

In tandem case, the flow structure is more complicated; more number of blades means more stagnation points and more areas of complex flows round the leading and trailing edges. Even, interaction of boundary layer of front and aft blades must be also considered as a challenging phenomenon. For these reasons, computational grids of tandem case are approximately 2 times the

grids of conventional case.

Table 6 Computational grids of tandem and conventional cases

		Number of nodes	Height layers	O-type layers	Tip layers
Tandem	Coarse r,s	149k,125k	30	10,5	4,-
	Medium r,s	510k,473k	50	16,11	7,-
	Fine r,s	1328k,1319k	80	21,17	11,-
Conv.	Coarse r,s	63k,47k	30	10,5	4,-
	Medium r,s	220k,172k	50	16,11	7,-
	Fine r,s	600k,501k	80	21,17	11,-

In order to ensure of the independency of the number of grids on the results of numerical, pressure distribution over the blades and mass flow rate at operating points near design points of both cases are undertaken by using all three sets of grids. Table 7 shows calculated mass flow rates. Obviously, the results do not change significantly from medium number of grids to fine grids. In fact, deviation of mass flow rate between medium and fine grids is less than 1% for both cases.

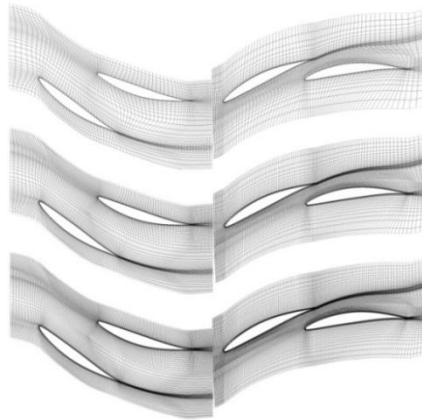


Fig. 14. Mid-span view of tandem case computational grids.

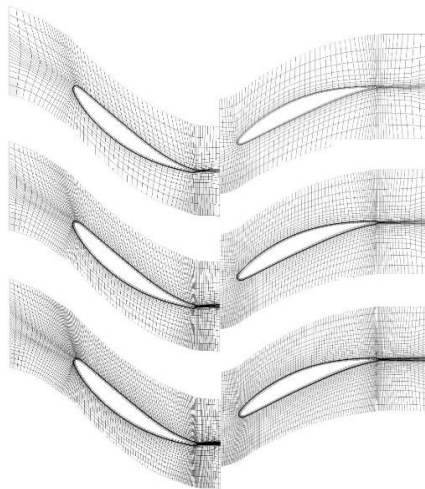


Fig. 15. Mid-span view of conventional case computational grids.

Table 7 Mass flow deviation in near design point

		mass flow	% deviation
Tandem	Coarse	27.6106	-
	Medium	28.2410	0.7984
	Fine	28.6623	0.4648
Conv.	Coarse	21.5732	-
	Medium	21.7373	1.2054
	Fine	21.9994	0.7606

Stream-wise Pressure distributions over the blades at mid-span radius of rotor and stator blades for all sets of grids are also computed and compared for both tandem and conventional cases. In both cases, results of medium and fine grids do not differ significantly and the points of maximum pressure near leading edge and minimum pressure over the suction surfaces are equal in both value and their locations. This comparison is demonstrated in fig. 16 for tandem rotor and mid-span radius.

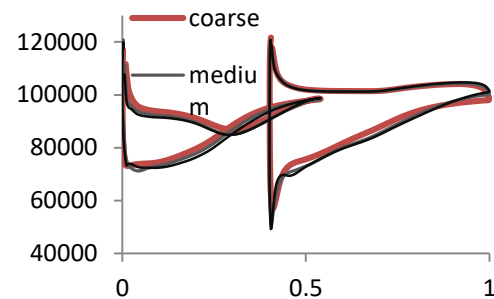


Fig. 16. Stream-wise pressure distribution on mid-span profile of tandem rotor.

7. RESULTS AND DISCUSSION

Having decided on the number of grids, Performance characteristic maps of tandem and conventional stages in 60%, 70%, 80%, 90%, 100% and 110% of design speed are computed. The results are primarily presented in the form of non-dimensional parameters of stage loading coefficient against flow coefficient (ψ - ϕ) in fig. 17.

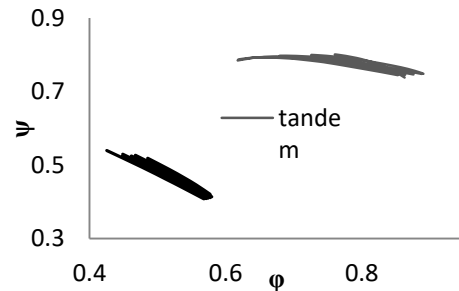


Fig. 17. Characteristic map of stage loading coefficient.

Both stages demonstrate nearly linear slope but the absolute value of slope is smaller for tandem case. The reason for such behavior is because, tandem and conventional stages are designed with similar blade loading parameters (DF and DH), but the resultant stage loading coefficient of tandem stage

will be inevitably larger than the conventional case; Since the gradient of stage loading coefficient (ψ) against flow coefficient (ϕ) relates to the decision on design stage loading coefficient (ψ_d) and design flow coefficient (ϕ_d) according to eq. (11) (Aungier, 2003), then it is quite natural to have lower gradients on ψ - ϕ diagram of tandem stage.

$$\frac{\partial \psi}{\partial \phi} = \frac{\psi_d - 1}{\phi_d} \quad (11)$$

This phenomenon causes the pressure ratio at various mass flow rates do not vary significantly which is considered as an advantage for tandem blades at off-design operation points. Whatever one can increase the stage loading at design point, the curves will be more flat.

It must be mentioned that some other issues such as sonic flow regime in the passage or nonlinear effects at stall region will also affect the slope of the characteristics curve which is not subject of this study.

Total to total pressure ratios, isentropic efficiencies and mass flow rates are figured and compared in fig. 18 and fig. 19.

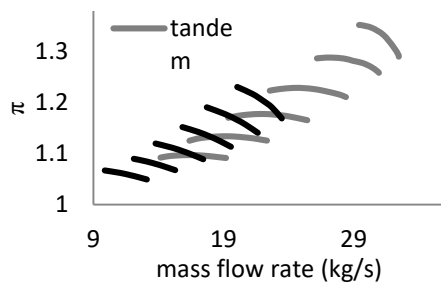


Fig. 18. Comparison of total to total pressure ratio vs. mass flow rate of compressor stages.

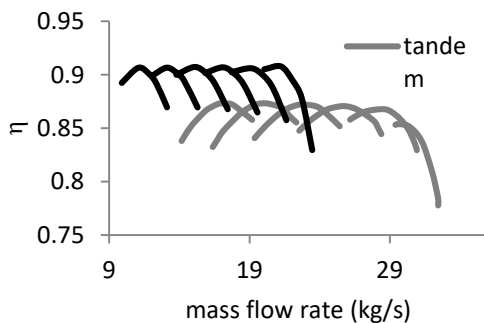


Fig. 19. Comparison of total to total isentropic efficiencies vs. mass flow rate of compressor stages.

Presenting characteristics curves in the forms of pressure ratio and efficiency against mass flow rate at 6 different shaft rotational speed provide some more details on the behavior of tandem stages. Figure 18 shows that gradients of pressure ratio of tandem stage are all lower than conventional stage. Besides gradients of tandem stage at lower speeds are more flat than at higher speeds. It is very interesting that, tandem stage provides much higher

ratio. In fact the design pressure ratio at design point for tandem stage is 9.3% higher than conventional stage. This is a very important result which is directly affecting the whole size of a compressor for a certain targeted pressure ratio. The disadvantage of tandem stage is the occurrence of surge point at higher mass flow rate. Table 8 shows the improvement of pressure ratio and mass flow increase at peak efficiency point of tandem stage with respect to conventional stage at various rotational speeds.

Table 8 Comparison of tandem and conventional stages

	60%	70%	80%	90%	100%	110%
%PR improvement	3.3	4.5	5.9	7.4	9.3	11.2
% \dot{m} improvement	53.4	53.6	50.65	51.2	47.7	39.1

In fig. 19 efficiency of the stages are presented for both stages. The penalty of higher pressure ratio is being paid in efficiency of tandem stage at various rotational speeds. Although the efficiency curves of tandem stage are more flat than conventional one, but they are lower at all speed lines. Table 9 reports stage performance parameters at peak efficiency point at design speed.

Table 9 Stage performance parameters in peak efficiency point

	Mass flow	π	η
Tandem	28.25	1.29	87%
Conv.	19.13	1.17	90%

Peak efficiency of tandem stage is approximately 3% less than conventional stage. The reasons are may be due to the more sources of loss in tandem passages. It worth saying that, having higher pressure ratio in tandem blades may provide regions of transonic flow which consequently is ended with shock waves. Bearing in mind that, similar blade profiles are used for both passages while tandem blades probably are faced with transonic flow at higher rotational speed. Surely, using profiles such as multi circular arc for tandem blades can improve the efficiency at such speeds. There are also some ambiguities on the interaction of jet and boundary layer between the tandem blades that should be modeled properly and it may be a source of more loss. Furthermore, having more blades in tandem stage means that at the end of each trailing edge a wake is generated which consequently affects the incidence angle on the leading edge of next blade. In such situation it is natural to lose efficiency; however, at peak efficiency point, tandem stage allows 48% more mass flow passes through the passage.

At this stage studying the flow field within the passage may assist us to gain more knowledge about what exactly happens in tandem stage.

Figure 20 and fig. 21 show contours of relative Mach number at design speed and at mid-span height of tandem and conventional cases.

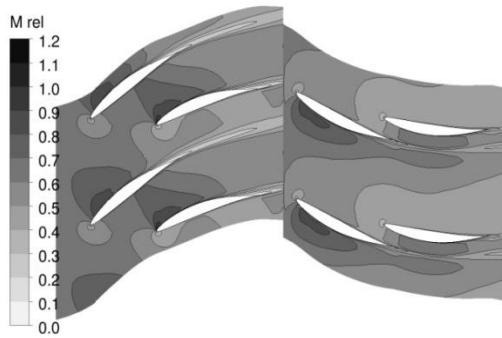


Fig. 20. Relative mach number contours in mid-span and design speed on tandem stage.

Obviously, maximum relative Mach number in tandem case is 1.1, while this parameter in conventional stage is at most 0.7. Therefore, higher level of loss in tandem stage is inevitable.

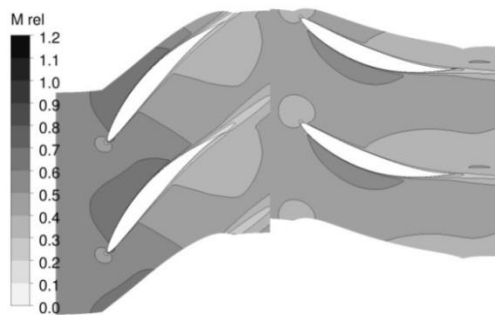


Fig. 21. Relative mach number contours in mid-span and design speed on conventional stage.

Even the generation of more regions of wake is apparently observed, which definitely vary the incidence angle in pitch wise direction. Perhaps one reason that instability point happens at higher mass flow is due to the irregular angle of incidence on aft blades. Naturally, the situation gets worse as flow passes through next blades. When the rotational speed increases to 110% of design speed, the situation is getting more critical, the maximum relative Mach number increases to 1.2 in tandem stage (fig. 22) and 0.8 in conventional stage (fig. 23) which provides a stronger shock structure over the suction surface of tandem rotor.

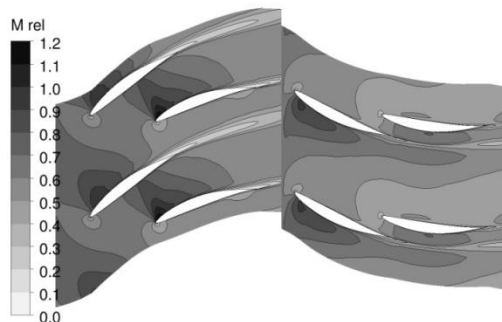


Fig. 22. Relative Mach number contours in mid-span and 110% design speed on tandem stage.

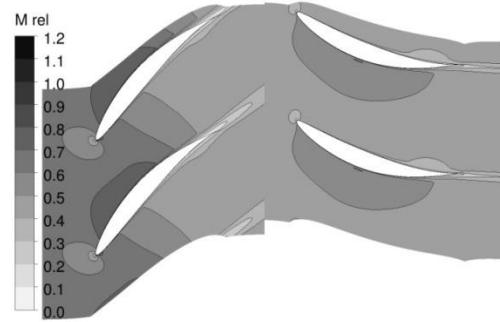


Fig. 23. Relative mach number contours in mid-span and 110% design speed on conventional stage.

It is interesting that, at higher span ratio such as 80%, the region of high Mach number expands and higher loss due to shock is generated (fig. 24). It means that, by marching toward the hub, flow velocity increases and the contribution of loss due to shock improves.

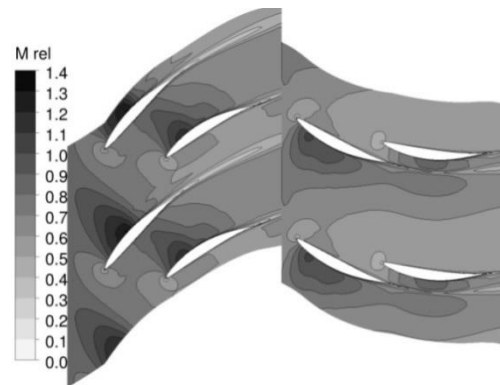


Fig. 24. Relative Mach number contours in 80%span and 110% design speed on tandem stage.

By increasing the pressure ratio and consequently Mach number in tandem passage of stator, the structure of jet and wake is getting more complex. In such situation, more attention is needed for proper modeling of mixing flow in this region. It may be required to use Large Eddy Simulation (LES) model to grasp a more accurate level of loss due to turbulence at these locations. It is also emphasized that, using suitable profile for the blades may improve the efficiency of tandem blades at high Mach numbers. It means that there are still rooms for earning better performance with lower level of deficiency.

8. CONCLUSION

Two stages of tandem and conventional compressors have been designed with similar blade loadings, but with different stage loading parameters. Also rotational speed, frontal area and axial width of both stages are similar. In the case of tandem blades, mass flow rate and pressure ratio are respectively 48% and 9.3% more than conventional case; on the other hand, it is resulted in about 3%

lower total to total isentropic efficiency. A highly loaded tandem stage demonstrates a flat characteristic map as non-dimensional stage loading coefficient which is plotted against flow coefficient (ψ vs. ϕ). Flat characteristic curves may be employed for the cases that equal pressure ratio are required at various mass flow rates. It is concluded that there are some options in design procedure to achieve higher pressure ratio with less loss and higher efficiency. It is also recommended that due to the nature of interaction of jet and wake and its resultant large scale eddies, using the capability of LES modeling may result in more accurate prediction of performance parameters.

REFERENCES

- Aungier, R. H (2003). *Axial-flow compressors: a strategy for aerodynamic design and analysis*, 1st Edition, ASME Press.
- Bammert, K. and H. Beelte (1980). Investigations of an axial flow compressor with tandem cascades. *Journal of Engineering for Power* 102(4),971-977.
- Brent, J. A. and D. R. Clemmons (1975). *Single-stage experimental evaluation of tandem-airfoil rotor and stator blading for compressors. Part VIII: Final report*. NASA CR-134713.
- Cheatham, J. G (1974). *Single-stage experimental evaluation of tandem-airfoil rotor and stator blading for compressors. Part VII: Data and performance for stage E*. NASA CR-134529.
- Fidalgo, V. J., C. A. Hall and Y. Colin (2012). A Study of Fan-Distortion Interaction within the NASA Rotor 67 Transonic Stage. *Journal of Turbomachinery* 134(5), 051011.
- Hathaway, M. D (1986). *Unsteady flows in a single-stage transonic axial-flow fan stator row*. NASA Technical Memorandum 88929.
- Hoeger, M., R. D. Baier and S. Fischer (2011). High turning compressor tandem cascade for high subsonic flows, Part 1: Aerodynamic Design. *47th AIAA/ASME/SAE/ASEE Joint Propulsion Conference & Exhibit* AIAA-2011-5601.
- McGlumphy, J., W. F. Ng, S. R. Wellborn and S. Kempf (2009). Numerical Investigation of Tandem Airfoils for Subsonic Axial-Flow Compressor Blades. *Journal of Turbomachinery* 131(2), 021018.
- McGlumphy, J., S. R. Wellborn, S. Kempf and W. F. Ng, (2010). 3D numerical investigation of tandem airfoils for a core compressor rotor. *Journal of Turbomachinery* 132(3), 031009.
- Müller, L., D. Kožulovi, D. Wulff, S. Fischer and U. Stark (2011). High Turning Compressor Tandem Cascade for High Subsonic Flows–Part 2: Numerical and Experimental Investigations. *AIAA/ASME/SAE/ASEE Joint Propulsion Conference & Exhibition*.
- Qiushi, L., W. Hong and Z. Sheng (2010). Application of tandem cascade to design of fan stator with supersonic inflow. *Chinese Journal of Aeronautics* 23(1), 9-14.
- Shen, C., X. Qiang and J. Teng (2012). Numerical and experimental investigation of an axial compressor flow with tandem cascade. *Journal of Thermal Science* 21(6), 500-508.
- Strazisar, A. J., J. R. Wood, M. D. Hathaway and K. L. Suder (1989). *Laser anemometer measurements in a transonic axial-flow fan rotor*. NASA Technical 2879.
- Suga, S., H. Hasegawa and A. Matsuoka (2003). Development of highly loaded fan with tandem cascade. *41st Aerospace Sciences Meeting and Exhibit*. 6-9 January 2003, Reno, Nevada, AIAA 2003-1065.
- Suga, S., A. Matsuoka, Y. Sakai and K. Hashimoto (2003). A Booster Stage with Tandem Cascade Rotor for Fan Engine. *Proceedings of the International Gas Turbine Congress*. 2-7 November, Tokyo, IGTC2003Tokyo TS-109.